ACS APPLIED MATERIALS & INTERFACES

Research Article

www.acsami.org

Stretchable and Reversibly Deformable Radio Frequency Antennas Based on Silver Nanowires

Lingnan Song,[†] Amanda C. Myers,[†] Jacob J. Adams,[‡] and Yong Zhu*,[†]

[†]Department of Mechanical and Aerospace Engineering, [‡]Department of Electrical and Computer Engineering, North Carolina State University, Raleigh, North Carolina 27695, United States

ABSTRACT: We demonstrate a class of microstrip patch antennas that are stretchable, mechanically tunable, and reversibly deformable. The radiating element of the antenna consists of highly conductive and stretchable material with screen-printed silver nanowires embedded in the surface layer of an elastomeric substrate. A 3-GHz microstrip patch antenna and a 6-GHz 2-element patch array are fabricated. Radiating properties of the antennas are characterized under tensile strain and agree well with the simulation results. The antenna is reconfigurable because the resonant frequency is a function of the applied tensile strain. The antenna is thus well suited for applications like wireless strain sensing. The material and fabrication technique reported here could be extended to achieve other types of stretchable antennas with more complex patterns and multilayer structures.

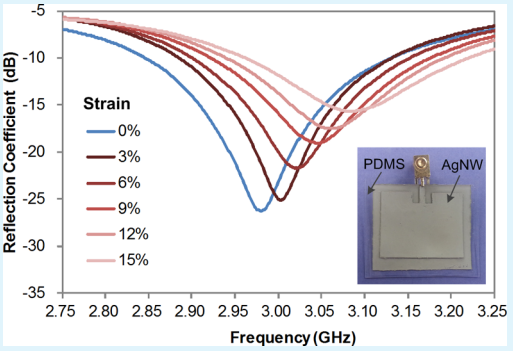

KEYWORDS: *silver nanowire, stretchable antenna, wireless strain sensing, printed electronics, microstrip patch antenna*

1. INTRODUCTION

Wearable systems for detecting human motions and monitoring human health/wellness have attracted significant attention in recent years. A variety of wearable sensors,[1,2] energy harvesting/storage,[3,4] and electronic circuits[5,6] have been developed, which represents exciting progress toward battery-less (or free) health monitoring. Wearable wireless communication is key to convey the sensory data and provide remote diagnosis, and a radio frequency antenna is a critical component for the wireless communication.

Antennas are conventionally fabricated by printing or etching metal patterns on rigid substrates, which can easily crease and even fail to function properly when subjected to mechanical deformation (e.g., stretching, folding, or twisting). Thus development of flexible, stretchable, and conformal antennas calls for new electronic materials and/or new device configurations. For example, flexible antennas have been realized by electroplating thin metal foils (e.g., copper[7] and gold[8]) on elastic dielectric substrates. 3D conformal antennas have been developed by printing silver nanoparticles on a 3D surface.[9] However, these antennas are not able to withstand tensile strain. Several types of stretchable antennas, including cone,[10] loop,[11] dipole,[12,13] and patch,[14] have been realized by encasing liquid metal alloys into stretchable microchannels. Such stretchable antennas can also be used as self-contained strain sensors.[15] This approach, however, is limited in terms of scalable manufacturing due to its fabrication complexity and potential problems caused by leakage of the liquid metals. Recently, stretchable antenna has also been achieved using carbon nanotube (CNT) sheet and polymer substrates.[16,17]

Silver nanowires (AgNWs) have emerged as a promising material for flexible/transparent[18,19] and stretchable electrodes[20] in a number of applications including light emitting diodes,[21] solar cells,[22] and wearable sensors.[23] In addition to flexible antennas,[24,25] AgNWs were recently used in fabricating stretchable antennas.[26] However, the antenna performances were not evaluated under tensile strain. In addition, the reversibility under stretching and other deformation modes was not demonstrated.

In this paper, we report a class of microstrip patch antennas that are stretchable, mechanically tunable, and reversibly deformable. The radiating element of the antenna consisted of a highly conductive and stretchable material with AgNWs embedded in the surface layer of an elastomeric substrate. More specifically, a 3-GHz microstrip patch antenna and a 6-GHz, 2-element patch array were fabricated. Radiating properties of the antennas were characterized under tensile strain and agreed well with the simulation results. Since the resonant frequency increased with increasing tensile strain, the antenna can be used for wireless strain sensing. Finally, the antennas were demonstrated to maintain the same spectral properties under severe bending, twisting, and rolling.

2. RESULTS AND DISCUSSION

Figure 1a shows the fabrication procedure for the AgNW/PDMS patch antennas. Two types of patch antennas – the single patch (Figure 1b) and 2-element array (Figure 1c) – were fabricated in this study using the same process. The thickness of the AgNW/PDMS layer is ~0.5 mm, and the

Received: December 25, 2013
Accepted: March 4, 2014
Published: March 4, 2014

   dx.doi.org/10.1021/am405972e | ACS Appl. Mater. Interfaces 2014, 6, 4248–4253

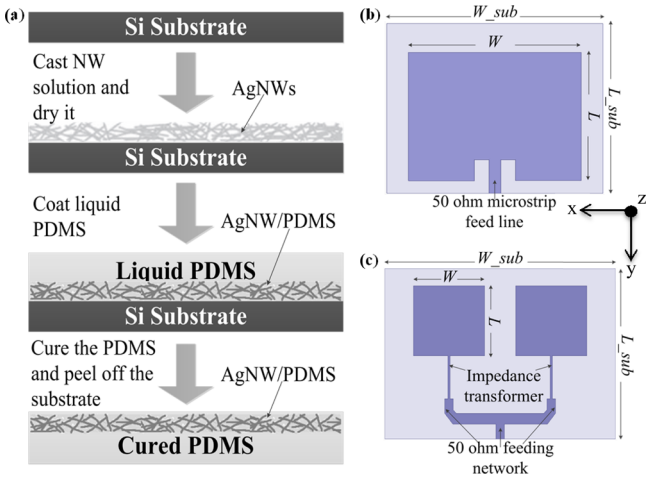

Figure 1. (a) Fabrication procedure for the AgNW/PDMS flexible patch antenna and the schematics for (b) microstrip patch antenna and (c) 2-element patch array.

separation between the radiating element and the ground plane is ~1 mm (±0.1 mm).

The single patch antenna consists of a rectangular radiating patch, a ground plane, and a uniform layer of dielectric substrate between them. Dimensions of the patch were designed based on the transmission-line model, which gives the width W and the length L as functions of the resonant frequency f_{res}, the relative permittivity of substrate material ε_r, and the thickness of substrate h[27] (see the Experimental Section).

The substrate material PDMS has a reported relative permittivity ranging from ε_r = 2.67 to 3.00 and loss tangent ranging from tanδ = 0.01 to 0.05 over an operating frequency range of 1.0 to 5.0 GHz.[14] Accordingly, we modeled the substrate material with relative permittivity of ε_r = 2.80 and loss tangent of tanδ = 0.02 for the 3-GHz application. Conductivity of the AgNW/PDMS stretchable conductor is ~8,130 S cm^{-1} before stretching.[20] Here we used a constant conductivity of 8,130 S cm^{-1} for the antenna considering the applied strains were relatively small.

To obtain the resonance frequency of 3 GHz, the rectangular patch was designed to be 36.0 mm × 29.2 mm, backed with a 45.0 mm × 40.0 mm ground plane. To match the input impedance with a 2.5 mm × 8.0 mm 50Ω microstrip feed line, the inset feeding method was employed, which left a 3 mm external part and eliminated the need for an external matching network. Length and width of the cutout inset region were optimized in ANSYS HFSS to achieve lower return loss and less additional coupling between patch and feed line.

The 6-GHz 2-element array patch antenna was designed similarly with the same material parameters except an increased loss tangent of tanδ = 0.05. Two identical radiating elements with dimensions shrinking to 18.0 mm × 14.3 mm were arranged in parallel and fed simultaneously by a feeding network. Since the doubled operating frequency renders the input impedance more sensitive to inaccuracy in dimensions, we changed the matching strategy by introducing an impedance transformer at the edge of each radiating element to reduce possible fabrication error. Note that due to the fabrication error, the obtained resonance frequencies for the patch and the 2-element array are 2.92 and 5.92 GHz, respectively.

Simulated radiation patterns of the one and two element antennas were obtained by far-field calculation in ANSYS HFSS, as shown in Figure 2. Simulation results for the radiation

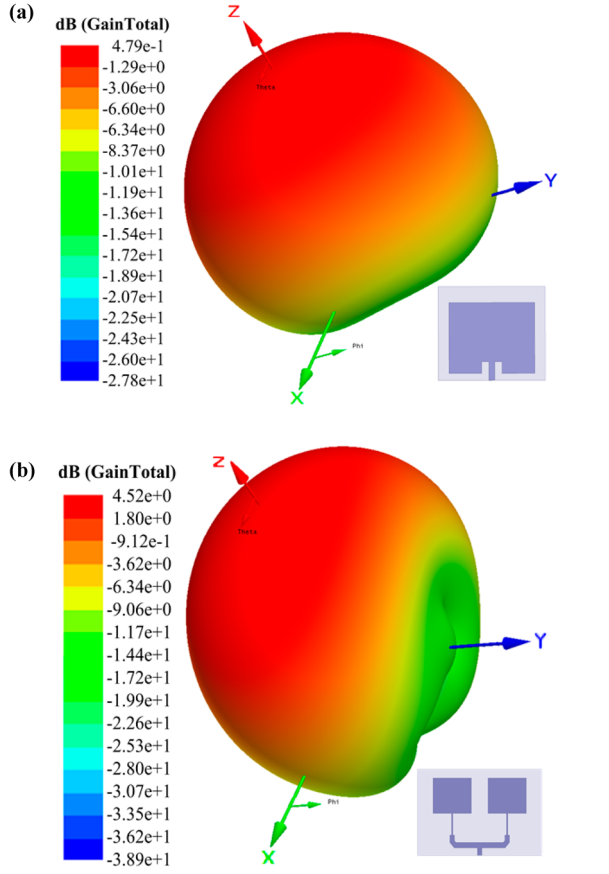

Figure 2. Simulated radiation pattern for the AgNW/PDMS (a) microstrip patch antenna and (b) 2-element patch array.

Table 1. Comparison of Simulated Radiation Properties for Microstrip Patch Antenna and 2-Element Patch Array

radiation properties	monopole patch	2-element patch array
resonant frequency	2.92 GHz	5.92 GHz
peak directivity	4.16 dBi	8.14 dBi
peak gain	0.37 dBi	4.90 dBi
radiation efficiency	41.83%	48.83%
bandwidth	88 MHz (3.0%)	330 MHz (5.5%)

properties of both antennas are summarized in Table 1 for comparison. The 2-element array, compared with the single element, increases the directivity by 4.5 dB and the fractional bandwidth by 2.5%, with higher radiation efficiency at the same time.

The patch antennas were characterized experimentally and compared to the simulated results. Measured and simulated frequency responses agreed very well, with the difference within the manufacturing imperfection and measurement uncertainty. Figure 3 shows the measured spectrum response of the reflection coefficient over a frequency range of 2 to 4 GHz for the single patch antenna before stretching, with S_{11} below −20 dB at the center frequency of 2.92 GHz and above −1 dB far

dx.doi.org/10.1021/am405972e | ACS Appl. Mater. Interfaces 2014, 6, 4248−4253

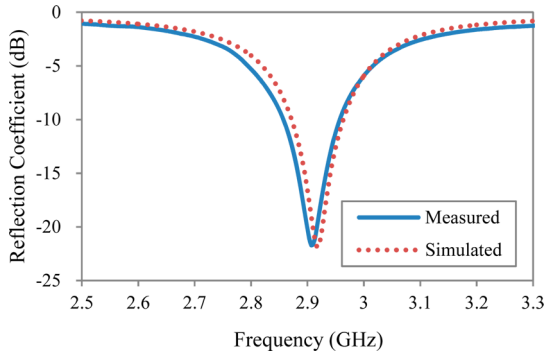

Figure 3. Comparison of measured (blue solid) and simulated (red dotted) reflection coefficient for the AgNW/PDMS microstrip patch antenna.

outside the operating region. The bandwidth, defined as the frequencies where $S_{11} < -10$ dB, was 97.5 MHz.

We compared the simulated reflection coefficient for the 2-element array to the measured reflection coefficient from 4 to 8 GHz. The array was initially designed with a single operating band at 6 GHz, while the measured results showed an additional operating band at around 5.3 GHz. We studied the mechanism of the unexpected resonance by introducing small dimension deviations due to possible fabrication errors compared to the antenna model with ideal dimensions. As is shown in Figure 4, when we assume that one of the radiating

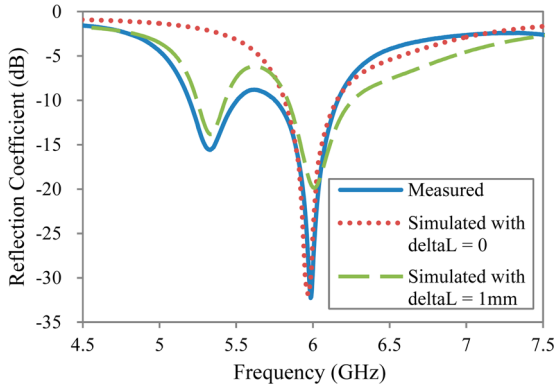

Figure 4. Comparison of measured (blue solid) and simulated reflection coefficient for the AgNW/PDMS 2-element patch array, with ideal dimensions (red dotted) and 1 mm deviation in length for one of the radiating elements (red dashed).

elements was fabricated larger in length than the other, the simulated frequency response would extend to the lower frequency band and form another band located at around 5.3 GHz for a 1 mm deviation in length, which was very close to what we observed experimentally.

Far-field performance for the single patch antenna was tested in an anechoic chamber. We measured the peak gain over frequency range of 2 to 4 GHz. Radiation efficiency was estimated using the measured gain and simulated directivity, which is compared to the simulated radiation efficiency in Figure 5. To further study loss mechanisms of the AgNW/PDMS patch antenna with respect to radiation efficiency, we modeled antennas composed of four combinations of dielectric substrates and metal materials. We considered both AgNW/PDMS conductor with conductivity of 8130 S cm^{-1} and perfect electric conductor (PEC) with infinite conductivity for the

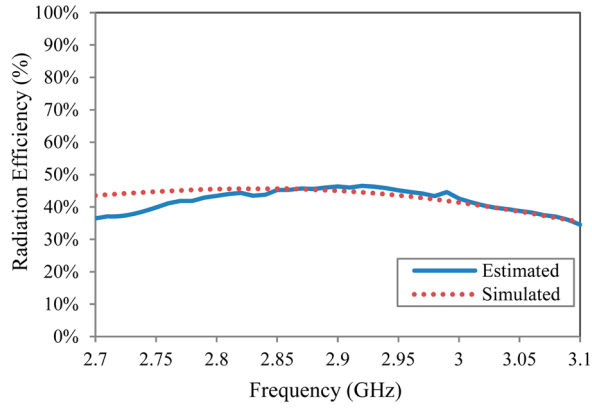

Figure 5. Estimated (blue solid) and simulated (red dotted) radiation efficiency for the microstrip patch antenna.

metal components. Also, we evaluated both PDMS with loss tangent of tanδ = 0.02 and lossless dielectric substrate. Table 2

Table 2. Comparison of Simulated Radiation Efficiency of Antennas in Different Dielectric and Metal Materials

substrate	metal	radiation efficiency
lossy PDMS	AgNW/PDMS	41.53%
lossy PDMS	PEC	55.76%
lossless material	AgNW/PDMS	67.20%
lossless material	PEC	100%

summarized the simulation results of radiation efficiency for all four combinations. Compared to the ideal configuration, radiation efficiency was decreased from 100% to around 56% by the lossy substrate and to around 67% by the AgNW/PDMS with finite conductivity. For completeness, the radiation pattern for the antenna in the E-plane and the H-plane is shown in Figure 6. The stretchable antenna exhibits excellent radiation properties as well as good agreement with the simulated results.

To test the mechanical tunability as a stretchable antenna, tensile strain ranging from 0% to 15% was applied to the AgNW/PDMS patch antenna in the width direction (perpendicular to the cable connection), while the reflection coefficient was collected by the network analyzer simultaneously. The antenna was tested on a custom-made mechanical testing stage, where all the components are made of insulators (e.g., ceramic, glass, and Teflon). Figure 7a shows the measured frequency response of the reflection coefficient under tensile strain from 0% to 15%. With the increasing strain, the spectrum response shifted to higher band, the center frequency increased almost linearly, and the −10 dB bandwidth remained higher than 80 MHz, as listed in Table 3. The results suggest that performance of the stretchable antenna was not largely compromised during stretching.

The strain was then decreased back to zero on the antenna. The center frequency was also measured during the releasing process. Upon complete release of the strain, the antenna returned to its original resonant frequency demonstrating excellent reversible deformability (Figure 7b).

To analyze the frequency shift due to the applied strain, we accounted for the changing dimensions as functions of the strain. PDMS is a typical hyperelastic material where the total volume is constant during deformation.[28] Therefore when the antenna is elongated in the width direction, the length and

dx.doi.org/10.1021/am405972e | ACS Appl. Mater. Interfaces 2014, 6, 4248−4253

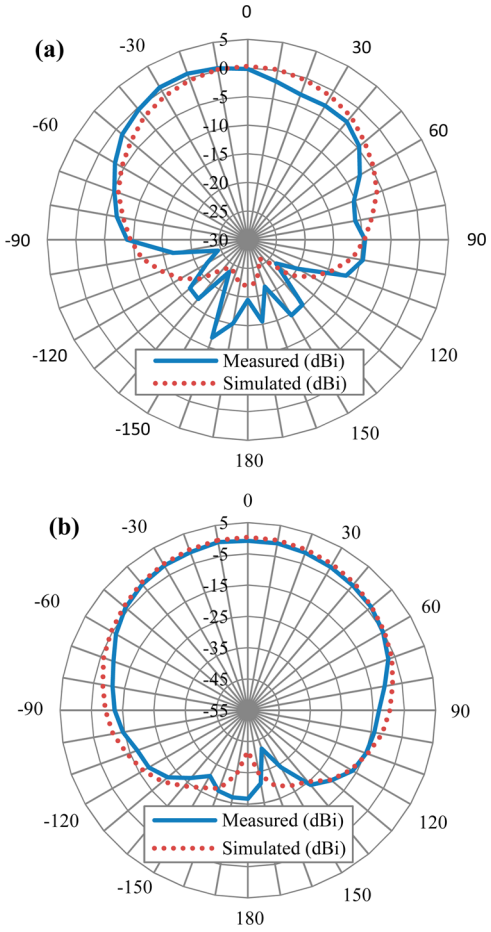

Figure 6. Measured (blue solid) and simulated (red dotted) normalized radiation pattern (a) in the E-plane and (b) in the H-plane for the microstrip patch antenna at frequency of 2.92 GHz.

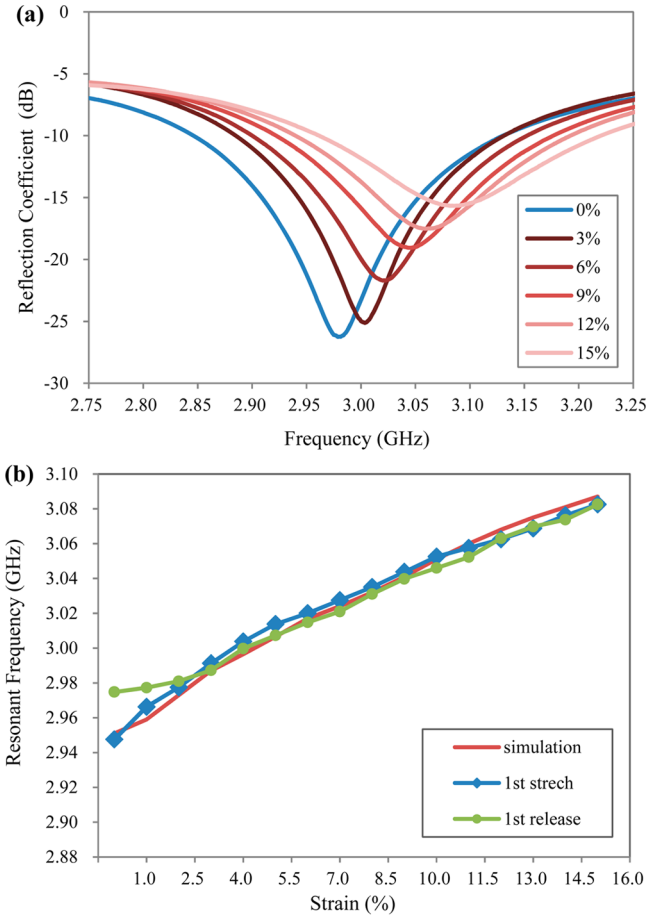

Figure 7. (a) Measured frequency response of reflection coefficient for the AgNW/PDMS microstrip patch antenna under tensile strains from 0% to 15%. (b) Comparison of simulated (red dotted) and measured resonant frequency during stretch (blue solid) and release (green solid) for the AgNW/PDMS microstrip patch antenna under tensile strain from 0% to 15%.

height shrink proportionally. The resonant frequency f_{res} is determined by the length of the radiating patch as

$$f_{res} = \frac{c}{2L\sqrt{\varepsilon_{reff}}} \tag{1}$$

where c is the speed of light in vacuum, L is the length of microstrip patch antenna, and ε_{reff} is the effective relative permittivity of the microstrip, to account for the differing permittivities of the air and substrate material (see the Experimental Section).

When a tensile strain of s is applied, the new dimensions of the antenna, patch width W, patch length L, and substrate thickness h as the function of s are

$$W = W_0(1 + s) \tag{2}$$

$$L = \frac{L_0}{\sqrt{1 + s}} \tag{3}$$

$$h = \frac{h_0}{\sqrt{1 + s}} \tag{4}$$

where W_0, L_0, and h_0 are the original dimensions before stretch, and for a small strain $s \ll 1$, the new resonant frequency is represented as

Table 3. Measured Resonant Frequency and Bandwidth of the AgNW/PDMS Microstrip Patch Antenna under Tensile Strains from 0% to 15%

strain (%)	0	3	6	9	12	15
resonant frequency (GHz)	2.947	2.991	3.020	3.044	3.063	3.083
bandwidth (MHz)	239	244	253	254	243	258

$$f_{res} = \frac{c\sqrt{1 + s}}{2L_0\sqrt{\varepsilon_{reff}}} \approx \frac{c}{2L_0\sqrt{\varepsilon_{reff}}}\left(1 + \frac{1}{2}s\right) \tag{5}$$

which gives a linear relationship between the resonant frequency f_{res} to the applied strain s. The effective dielectric constant ε_{reff} was updated for each strain level.

Results are compared to measurements during both stretching and releasing processes in Figure 7b. The recorded center frequency as a function of tensile strain agrees well with what is predicted by modeling. The difference between simulated and measured resonant frequencies is within ±3 MHz at each point, which is relatively insignificant (within ±0.2%). The stretchable antenna is thus well suited for wireless strain sensing applications.

dx.doi.org/10.1021/am405972e | ACS Appl. Mater. Interfaces 2014, 6, 4248−4253

To further demonstrate the reversible deformability of our antennas, they were subjected to other deformation modes including bending, twisting, and rolling, as shown in Figure 8.

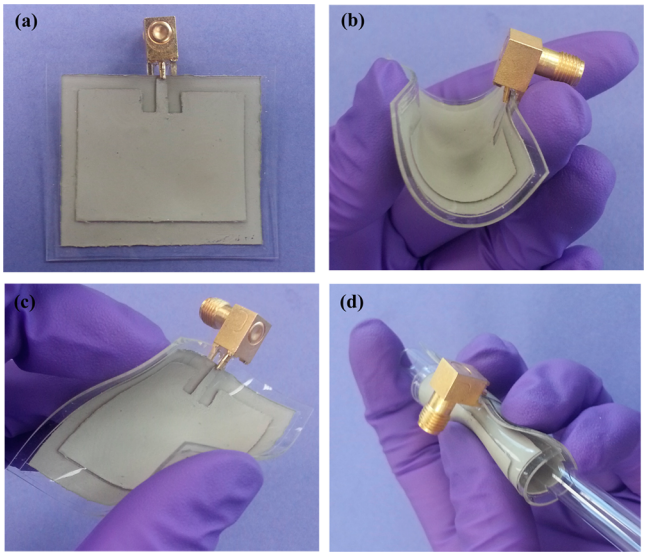

Figure 8. Photographs of a stretchable microstrip patch antenna composed of AgNW/PDMS flexible conductor: (a) relaxed, (b) bent, (c) twisted, and (d) rolled.

The antenna was deformed by bending by 90° along the long axis, twisting along the long axis, rolling on both axes. After the deformed antenna was returned to its original state, it maintained almost the same spectral properties with difference of the resonant frequencies within ±1 MHz (<0.1%) before and after deformation in each case, which demonstrates that the AgNW/PDMS flexible antenna is reversibly deformable and robust.

3. CONCLUSION

We have demonstrated a class of microstrip patch antennas that are stretchable, mechanically tunable, and reversibly deformable. A 3-GHz patch antenna and a 6-GHz 2-element patch array were fabricated. Radiating properties of the antennas were characterized under tensile strain, which agreed well with the simulation results. The antenna was mechanically tunable, enabling the resonant frequency to change as a function of the applied tensile strain. Thus it was well suited for applications like wireless strain sensing. The radiation efficiency was limited by losses in both the PDMS substrate and AgNW. The antennas were also demonstrated to maintain the same spectral properties after severe bending, twisting, and rolling. The material and fabrication technique reported here could be extended to achieve other types of stretchable antennas with more complex patterns and multilayer structures.

EXPERIMENTAL SECTION

Fabrication Process. AgNWs with an average diameter of ~90 nm and length in the range of 10−60 μm were synthesized in solution (from Blue Nano).[20] They are dispersed in ethanol with a concentration of 10 mg/mL. As shown in Figure 1a, the antenna pattern was cut out from a stencil mask on a precleaned substrate such as silicon (Si) wafer. AgNWs solution was drop casted into the mask on top of a hot plate (set at 55 °C) and then dried to form a conductive film of AgNWs with the desired antenna pattern. After peeling off the stencil mask, liquid PDMS was casted on top of the AgNW film and heated at 100 °C for 1 h to cure. When the cured PDMS layer was peeled off the substrate, the AgNW film was embedded into the PDMS forming a surface layer both conductive and stretchable. Fabrication of the ground plane layer followed the same procedure and then bonded with the patch layer before the liquid PDMS cured.

Modeling and Design. The width W and the length L are designed based on the transmission-line model[27]

$$W = \frac{c}{2f_{\text{res}}}\sqrt{\frac{2}{\varepsilon_r + 1}} \tag{6}$$

$$L = \frac{c}{2f_{\text{res}}\sqrt{\varepsilon_{\text{reff}}}} - 2\Delta L \tag{7}$$

where

$$\varepsilon_{\text{reff}} = \frac{\varepsilon_r + 1}{2} + \frac{\varepsilon_r - 1}{2}\left[1 + 12\frac{h}{W}\right]^{-1/2} \tag{8}$$

$$\Delta L = 0.412h\frac{(\varepsilon_{\text{reff}} + 0.3)\left(\frac{W}{h} + 0.264\right)}{(\varepsilon_{\text{reff}} - 0.258)\left(\frac{W}{h} + 0.8\right)} \tag{9}$$

with ΔL as the "extended" length at each end because fringing fields at the patch edges make the length appear larger electrically than physically. For low frequencies (<10 GHz) the effective dielectric constant is essentially constant, referred to as the static values and given by eq 8. Equation 9 is a common approximate relation for the extension of length depending on the effective dielectric constant $\varepsilon_{\text{reff}}$ and the width-to-height ratio (W/h). Typically $\Delta L \ll L$.

Antenna Measurement. An antenna was connected to a coaxial cable by a SMA connector. S-parameters were collected using an Agilent E5071C Vector Network Analyzer to measure the resonant frequency and reflection coefficient. Radiation patterns were measured in the anechoic chamber at the NC State Remote Educational Antenna Lab (REAL). 2D pattern cuts were measured in the orthogonal E- and H-planes (YZ and XZ planes). Each cut was obtained by rotating the antenna under test (AUT) in 10 degree increments while recording the received signal with a broadband horn antenna (A.H. Systems) to produce the relative pattern plot. Absolute gain was calculated via gain comparison to a standard gain horn (A.H. Systems). The results given in the paper represent the copolar radiation patterns and gain.

AUTHOR INFORMATION

Corresponding Author

*E-mail: yong_zhu@ncsu.edu.

Notes

The authors declare no competing financial interest.

ACKNOWLEDGMENTS

This work was supported in part by the National Science Foundation through the EFRI program (EFRI-1240438) and ASSIST Engineering Research Center at NCSU (EEC-1160483). The authors would like to thank Dr. Michael Dickey for providing access to their custom-made mechanical testing stage. L.S. is grateful to the Global Engagement in Academic Research (GEAR) Program at NCSU.

REFERENCES

(1) Kim, D.-H.; Lu, N.; Ma, R.; Kim, Y.-S.; Kim, R.-H.; Wang, S.; Wu, J.; Won, S. M.; Tao, H.; Islam, A.; Yu, K. J.; Kim, T.; Chowdhury, R.; Ying, M.; Xu, L.; Li, M.; Chung, H.-J.; Keum, H.; McCormick, M.; Liu, P.; Zhang, Y.-W.; Omenetto, F. G.; Huang, Y.; Coleman, T.; Rogers, J. A. Epidermal Electronics. *Science* **2011**, 333, 838−843.

(2) Lipomi, D. J.; Vosgueritchian, M.; Tee, B. C.-K.; Hellstrom, S. L.; Lee, J. A.; Fox, C. H.; Bao, Z. Skin-Like Pressure and Strain Sensors

Based on Transparent Elastic Films of Carbon Nanotubes. *Nat. Nanotechnol.* **2011**, 788−792.
(3) Lee, M.; Chen, C.-Y.; Wang, S.; Cha, S. N.; Park, Y. J.; Kim, J. M.; Chou, L.-J.; Wang, Z. L. A Hybrid Piezoelectric Structure for Wearable Nanogenerators. *Adv. Mater.* **2012**, *24*, 1759−1764.
(4) Yu, C.; Masarapu, C.; Rong, J.; Wei, B.; Jiang, H. Stretchable Supercapacitors Based on Buckled Single-Walled Carbon-Nanotube Macrofilms. *Adv. Mater.* **2009**, *21*, 4793−4797.
(5) Sekitani, T.; Zschieschang, U.; Klauk, H.; Someya, T. Flexible Organic Transistors and Circuits with Extreme Bending Stability. *Nat. Mater.* **2010**, *9*, 4−6.
(6) Artukovic, E.; Kaempgen, M.; Hecht, D. S.; Roth, S.; Grüner, G. Transparent and Flexible Carbon Nanotube Transistors. *Nano Lett.* **2005**, *5*, 757−760.
(7) Lin, C.; Chang, C.; Cheng, Y. T.; Member, S.; Jou, C. F. Development of a Flexible SU-8/PDMS-Based Antenna. *IEEE Antennas Wireless Propag. Lett.* **2011**, *10*, 1108−1111.
(8) Hage-ali, S.; Tiercelin, N.; Coquet, P.; Sauleau, R.; Pernod, P.; Scientifique, C. Millimeter-Wave Patch Array Antenna on Ultra Flexible Micromachined Polydimethylsiloxane (PDMS) Substrate. *Antennas Propag. Soc. Int. Symp.* **2009**, *1*, 5−8.
(9) Adams, J. J.; Duoss, E. B.; Malkowski, T. F.; Motala, M. J.; Ahn, B. Y.; Nuzzo, R. G.; Bernhard, J. T.; Lewis, J. A. Conformal Printing of Electrically Small Antennas on Three-Dimensional Surfaces. *Adv. Mater.* **2011**, *23*, 1335−40.
(10) Cheng, S.; Member, S.; Wu, Z.; Hallbjörner, P.; Hjort, K. Foldable and Stretchable Liquid Metal Planar Inverted Cone Antenna. *IEEE Trans. Antennas Propag.* **2009**, *57*, 3765−3771.
(11) Cheng, S.; Rydberg, A.; Hjort, K.; Wu, Z. Liquid Metal Stretchable Unbalanced Loop Antenna. *Appl. Phys. Lett.* **2009**, *94*, 144103.
(12) So, J.-H.; Thelen, J.; Qusba, A.; Hayes, G. J.; Lazzi, G.; Dickey, M. D. Reversibly Deformable and Mechanically Tunable Fluidic Antennas. *Adv. Funct. Mater.* **2009**, *19*, 3632−3637.
(13) Kubo, M.; Li, X.; Kim, C.; Hashimoto, M.; Wiley, B. J.; Ham, D.; Whitesides, G. M. Stretchable Microfluidic Radiofrequency Antennas. *Adv. Mater.* **2010**, *22*, 2749−2752.
(14) Hayes, G. J.; Qusba, A.; Dickey, M. D.; Lazzi, G. Flexible Liquid Metal Alloy (EGaIn) Microstrip Patch Antenna. *IEEE Trans. Antennas Propag.* **2012**, *60*, 2151−2156.
(15) Cheng, S.; Wu, Z. A Microfluidic, Reversibly Stretchable, Large-Area Wireless Strain Sensor. *Adv. Funct. Mater.* **2011**, *21*, 2282−2290.
(16) Zhou, Y.; Bayram, Y.; Dai, L.; Volakis, J. L. Conformal Load-Bearing Polymer-Carbon Nanotube Antennas and RF Front-Ends. *Proc. IEEE Antennas Propag. Soc. Int. Symp.* **2009**, 1−4.
(17) Zhou, Y.; Bayram, Y.; Member, S.; Du, F.; Dai, L.; Volakis, J. L. Polymer-Carbon Nanotube Sheets for Conformal Load Bearing Antennas. *IEEE Trans. Antennas Propag.* **2010**, *58*, 2169−2175.
(18) Lee, J. Y.; Connor, S. T.; Cui, Y.; Peumans, P. Solution-Processed Metal Nanowire Mesh Transparent Electrodes. *Nano Lett.* **2008**, *8*, 689−692.
(19) De, S.; Higgins, T. M.; Lyons, P. E.; Doherty, E. M.; Nirmalraj, P. N.; Blau, W. J.; Boland, J. J.; Coleman, J. N. Silver Nanowire Networks as Flexible, Tranparent, Conducting Films: Extremely High DC to Optical Conductivity Ratios. *ACS Nano* **2009**, *3*, 1767−1774.
(20) Xu, F.; Zhu, Y. Highly Conductive and Stretchable Silver Nanowire Conductors. *Adv. Mater.* **2012**, *24*, 5117−5122.
(21) Yu, Z.; Niu, X.; Liu, Z.; Pei, Q. Intrinsically Stretchable Polymer Light-Emitting Devices Using Carbon Nanotube-Polymer Composite Electrodes. *Adv. Mater.* **2011**, *23*, 3989−3994.
(22) Yu, Z.; Li, L.; Zhang, Q.; Hu, W.; Pei, Q. Silver Nanowire-Polymer Composite Electrodes for Efficient Polymer Solar Cells. *Adv. Mater.* **2011**, *23*, 4453−4457.
(23) Yao, S.; Zhu, Y. Wearable Multifunctional Sensors using Printed Stretchable Conductors made of Silver Nanowires. *Nanoscale* **2014**, *6*, 2345−2352.
(24) Nogi, M.; Komoda, N.; Otsuka, K.; Suganuma, K. Foldable Nanopaper Antennas for Origami Electronics. *Nanoscale* **2013**, *5*, 4395−4399.
(25) Komoda, N.; Nogi, M.; Suganuma, K.; Kohno, K.; Akiyamac, Y.; Otsukac, K. Printed Silver Nanowire Antennas with Low Signal Loss at High-Frequency Radio. *Nanoscale* **2012**, *4*, 3148−3153.
(26) Rai, T.; Dantes, P.; Bahreyni, B.; Kim, W. S. A Stretchable RF Antenna with Silver Nanowires. *IEEE Electron Device Lett.* **2013**, *34*, 544−546.
(27) Balanis, C. A. *Antenna Theory: Analysis and Design*, 3rd ed.; Wiley: Hoboken, NJ, 2005; Chapter 14, pp 816−820.
(28) Xu, F.; Durham, J. D.; Wiley, B. J.; Zhu, Y. Strain-Release Assembly of Nanowires on Stretchable Substrates. *ACS Nano* **2011**, *5*, 1556−1563.